

Spin nematic phases in models of correlated electron systems: a numerical study

S. Capponi¹ and F. F. Assaad²

¹Laboratoire de Physique Théorique, CNRS UMR 5152,
Université Paul Sabatier, F-31062 Toulouse, France.

²Institut für Theoretische Physik und Astrophysik,
Universität Würzburg, Am Hubland, D-97074 Würzburg, Germany

(Dated: May 25, 2019)

Strongly interacting systems are known to often spontaneously develop exotic ground states under certain conditions. For instance, spin nematic phases have been discovered in various magnetic models. Such phases, which break spin symmetry but have no net local magnetization, have also been proposed by Nersesyan *et al.*¹ in the context of electronic models. We introduce a N -flavor microscopic model that interpolates from the large- N limit, where mean-field is valid and such a nematic phase occurs, to the more realistic $N = 1$ case. By using a sign-free quantum Monte-Carlo, we show the existence of a spin nematic phase (analogous to a spin flux phase) for finite N ; when N decreases, quantum fluctuations increase and this phase ultimately disappears in favor of an s-wave superconducting state. We also show that this nematic phase extends up to a finite critical charge doping.

Dynamical studies allow us to clarify the Fermi surface property : in the nematic phase at half-filling, it consists of 4 points and the low-energy structure has a Dirac cone-like shape. Under doping, we observe clear signatures of Fermi pockets around these points.

This is one of the few examples where numerical simulations show how quantum fluctuations can destroy a large- N phase.

PACS numbers: 71.27.+a71.10.Fd

I. INTRODUCTION

Spin nematic phases are characterized by an absence of local magnetic moment and long range orientational ordering of the spin degrees of freedom. Such phases were first introduced by Andreev and Grishchuk² and then discovered in several magnetic models^{3,4}. Recently, spin nematic phases have also attracted attention in the the context of cold atoms where a gas bose condensate of ⁵²Cr atoms in magnetic trap has been realized⁵. Due to the high spin, $J = 3$, of the ⁵²Cr atoms, it has been suggested that, upon release of the spin degrees of freedom, spin nematic states can be realized^{6,7}. Mean-field realization of spin-nematic phases in particle-hole symmetric fermionic models on a square lattice have equally been proposed by Nersesyan *et al.*¹. Those phases are characterized by a checkerboard pattern of *alternating spin currents* around elementary plaquettes, and are coined spin flux phases (SFP). They break $SU(2)$ spin symmetry as well as the lattice symmetry, but conserve time reversal symmetry. Such a phase could also possibly occur in an extended Hubbard model⁸. The goal of this paper is to provide a *microscopic* realization of SFP.

In this article, we concentrate on fermionic models on a square lattice and investigate the stability of the spin-flux phase. To do so, we consider the multi-flavored model Hamiltonian:

$$H = -t \sum_{\langle i,j \rangle, \alpha} \left(c_{i,\alpha}^\dagger c_{j,\alpha} + h.c. \right) - \frac{g}{2N} \sum_{\langle i,j \rangle} \left(\sum_{\alpha} i c_{i,\alpha}^\dagger \vec{\sigma} c_{j,\alpha} - i c_{j,\alpha}^\dagger \vec{\sigma} c_{i,\alpha} \right)^2. \quad (1)$$

Here, the sum runs over nearest neighbors on a two-dimensional square lattice. The spinors $c_{i,\alpha}^\dagger = \left(c_{i,\uparrow,\alpha}^\dagger, c_{i,\downarrow,\alpha}^\dagger \right)$ where α ranges from 1 to N . In the limit $N \rightarrow \infty$, the saddle point approximation becomes exact, and we recover the mean-field results of Ref. 1. As N is reduced, quantum fluctuations around this saddle point are progressively taken in account and ultimately at $N = 1$ we recover a spin-1/2 fermionic Hamiltonian. As we will see, the model, of Eq. (1) allows sign free auxiliary field quantum Monte Carlo (QMC) simulations for arbitrary band fillings and values of N . Hence, we can map out the phase diagram as a function of doping for various N , at fixed choice of coupling constant g/t . In the following, we fix $t = 1$ as the energy unit.

The article is organized as follows. In the next section, we briefly describe the path integral formulation of the partition function which is the basis of the mean field and quantum Monte Carlo simulations. In section III we present our numerical results which allow us to map out the phase diagram as a function of N and doping for a fixed coupling strength. Finally, we summarize our results in section IV.

II. MEAN-FIELD AND QUANTUM MONTE CARLO SIMULATIONS.

Both the saddle point equations and the QMC simulations are based on a path integral formulation of the partition function. Carrying out a Trotter breakup of the kinetic and interaction terms as well as a Hubbard-Stratonovitch transformation for the interaction term,

the partition function reads:

$$\begin{aligned}
Z &\simeq \int \underbrace{\prod_{\langle i,j \rangle, \tau} d\vec{\Phi}_{\langle i,j \rangle}(\tau)}_{\equiv D\vec{\Phi}} e^{-\sum_{\langle i,j \rangle, \tau} \vec{\Phi}_{\langle i,j \rangle}^2(\tau)/2} \text{Tr} \left[\prod_{\tau} e^{t\Delta\tau \sum_{\langle i,j \rangle, \alpha} (c_{i,\alpha}^\dagger c_{j,\alpha} + h.c.)} \right. \\
&\quad \left. e^{\sqrt{\Delta\tau g/N} \sum_{\langle i,j \rangle} \vec{\Phi}_{\langle i,j \rangle}(\tau) \cdot \left(\sum_{\alpha} ic_{i,\alpha}^\dagger \vec{\sigma} c_{j,\alpha} - ic_{j,\alpha}^\dagger \vec{\sigma} c_{i,\alpha} \right)} \right] = \\
&\int D\vec{\Phi} e^{-\sum_{\langle i,j \rangle, \tau} \vec{\Phi}_{\langle i,j \rangle}^2(\tau)/2} \text{Tr} \left[\prod_{\tau} e^{t\Delta\tau \sum_{\langle i,j \rangle} (c_i^\dagger c_j + h.c.)} e^{\sqrt{\Delta\tau g/N} \sum_{\langle i,j \rangle} \vec{\Phi}_{\langle i,j \rangle}(\tau) \cdot (ic_i^\dagger \vec{\sigma} c_j - ic_j^\dagger \vec{\sigma} c_i)} \right]^N \quad (2)
\end{aligned}$$

where $c_i^\dagger = (c_{i,\uparrow}^\dagger, c_{i,\downarrow}^\dagger)$. Note that in the last equation, the trace runs over a single flavor.

As is well known, in the large N limit the mean-field solution is recovered. With the substitution

$$\vec{\eta}_{\langle i,j \rangle}(\tau) = \frac{1}{\sqrt{N\Delta\tau g}} \vec{\Phi}_{\langle i,j \rangle}(\tau) \quad (3)$$

one obtains

$$\begin{aligned}
Z &\simeq \int D\vec{\eta} e^{-NS(\eta)} \quad (4) \\
S(\eta) &= \sum_{\langle i,j \rangle, \tau} \Delta\tau g \vec{\eta}_{\langle i,j \rangle}^2(\tau)/2 - \ln \text{Tr} \prod_{\tau} e^{t\Delta\tau \sum_{\langle i,j \rangle} (c_i^\dagger c_j + h.c.)} e^{\Delta\tau g \sum_{\langle i,j \rangle} \vec{\eta}_{\langle i,j \rangle}(\tau) \cdot (ic_i^\dagger \vec{\sigma} c_j - ic_j^\dagger \vec{\sigma} c_i)}
\end{aligned}$$

In this large N limit, the integral over the the fields η is dominated by the saddle point configuration and fluctuations around the saddle point are negligible. Moreover, by neglecting the τ dependence of the Hubbard-Stratonovitch fields, one obtains :

$$\begin{aligned}
S(\eta) &= \beta g \sum_{\langle i,j \rangle} \vec{\eta}_{\langle i,j \rangle}^2/2 - \ln \text{Tr} e^{-\beta H_{MF}(\eta)} \\
H_{MF}(\eta) &= -t \sum_{\langle i,j \rangle} (c_i^\dagger c_j + h.c.) \\
&\quad -g \sum_{\langle i,j \rangle} \vec{\eta}_{\langle i,j \rangle} \cdot (ic_i^\dagger \vec{\sigma} c_j - ic_j^\dagger \vec{\sigma} c_i) \quad (5)
\end{aligned}$$

and the saddle-point equations read :

$$\frac{\partial S(\eta)}{\partial \vec{\eta}_{\langle i,j \rangle}} = 0 \quad (6)$$

which correspond precisely to the mean-field solution¹

$$\vec{\eta}_{\langle i,j \rangle} = \langle ic_i^\dagger \vec{\sigma} c_j - ic_j^\dagger \vec{\sigma} c_i \rangle_{H_{MF}} \quad (7)$$

A. Staggered spin flux mean field solution

We consider the restricted order parameter:

$$\vec{\eta}_{\langle i,j \rangle} = \eta(-1)^{i_x+i_y} (\delta_{j-i, a_x} - \delta_{j-i, a_y}) \vec{e}_z. \quad (8)$$

This choice is certainly valid at half-band filling where perfect nesting pins the dominant instabilities to the wave vector $\vec{Q} = (\pi, \pi)$. Away from half-filling, order parameters at incommensurate wave vectors may be favorable. This is not taken into account in the present Ansatz. With the above form, the mean-field Hamiltonian reads:

$$H_{MF} = \sum_{\vec{k} \in MBZ, \sigma} \left(c_{\vec{k}, \sigma}^\dagger, c_{\vec{k}+\vec{Q}, \sigma}^\dagger \right) \begin{pmatrix} \varepsilon(\vec{k}) - \mu & -\sigma g \eta z(\vec{k}) \\ -\sigma g \eta z(\vec{k}) & \varepsilon(\vec{k} + \vec{Q}) - \mu \end{pmatrix} \begin{pmatrix} c_{\vec{k}, \sigma} \\ c_{\vec{k}+\vec{Q}, \sigma} \end{pmatrix} \quad (9)$$

where the sum over \vec{k} is restricted to the magnetic Brillouin zone (MBZ) and with

$$z(\vec{k}) = -2i (\sin(k_x + Q_x/2) - \sin(k_y + Q_y/2)) \quad (10)$$

Thus, we obtain the saddle point equation

$$\eta = \frac{1}{2L^2} \sum_{\vec{k} \in MBZ, \sigma} \left\langle \left(c_{\vec{k}, \sigma}^\dagger, c_{\vec{k}+\vec{Q}, \sigma}^\dagger \right) \begin{pmatrix} 0 & \sigma z(\vec{k}) \\ \sigma z(\vec{k}) & 0 \end{pmatrix} \begin{pmatrix} c_{\vec{k}, \sigma} \\ c_{\vec{k}+\vec{Q}, \sigma} \end{pmatrix} \right\rangle \quad (11)$$

which we solve self-consistently.

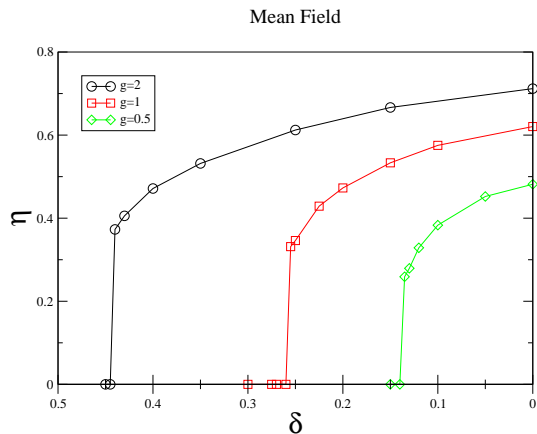


FIG. 1: (Color online) Mean Field order parameter as a function of band-filling for various coupling strengths g .

Figure 1 shows the order parameter as a function of doping. The staggered spin flux phase survives up to a finite critical doping, where a first order transition to the paramagnetic phase occurs. This transition is signaled by a jump in the order parameter. At half-band filling, the single particle dispersion relation is given by,

$$E(\vec{k}) = \pm \sqrt{\varepsilon^2(\vec{k}) + \Delta^2(\vec{k})} \quad (12)$$

with $\Delta(\vec{k}) = 2g\eta (\cos(k_x) - \cos(k_y))$. Hence, it exhibits Dirac cones around the $(\pm\pi/2, \pm\pi/2)$ k -points and the Fermi surface is given by those four points. In the doping range where the order parameter does not vanish the Fermi surface consists of hole-pockets centered around the above mentioned \vec{k} -points (See Fig. 2). Note that due to the d-wave symmetry of the order parameter, the Fermi surface is not invariant under reflections across the

$(1, 1)$ axis (i.e. $k_x \rightarrow k_y$ and $k_y \rightarrow k_x$). As appropriate for a first order transition, the Fermi surface changes abruptly from hole pockets around $(\pi/2, \pi/2)$ in the spin flux phase to a large Fermi surface centered around $(0, 0)$ in the paramagnetic phase.

B. Quantum Monte-Carlo

The Hamiltonian occurring in (4) is quadratic in the fermionic variables so that the trace can be carried out analytically to obtain:

$$Z \simeq \int D\vec{\Phi} e^{-\sum_{\langle i,j \rangle, \tau} \vec{\Phi}_{\langle i,j \rangle}^2(\tau)/2} [\det M(\Phi)]^N \quad (13)$$

Since the spin current is even under time reversal symmetry, it has been shown that, when $g \geq 0$, the fermionic determinant is positive for each Hubbard-Stratonovitch configuration⁹. This absence of sign problem is valid for any lattice topology and any filling. Hence each configuration of Hubbard Stratonovitch fields can be sampled according to its weight with Monte Carlo techniques.

In the following, we study the ground-state properties of the Hamiltonian (1) with the projector auxiliary field QMC algorithm on a two-dimensional square lattice. The details on this algorithm can be found for example in Ref. 10, where the authors consider a very similar model from the technical point of view. Dynamical information is obtained by using a recent implementation of the stochastic analytical continuation^{11,12}.

III. NUMERICAL RESULTS

A. Phase diagram

For $N = 1$, the interaction term of our model can be rewritten, up to a constant as:

$$\begin{aligned} & - \frac{g}{2} \sum_{\langle i,j \rangle} \left(\sum_{\alpha} i c_{i,\alpha}^\dagger \vec{\sigma} c_{j,\alpha} - i c_{j,\alpha}^\dagger \vec{\sigma} c_{i,\alpha} \right)^2 \\ & = - 3g \sum_{\langle i,j \rangle} (c_{i,\uparrow}^\dagger c_{i,\downarrow}^\dagger c_{j,\downarrow} c_{j,\uparrow} + h.c.) \\ & + \frac{3}{2}g \sum_{\langle i,j \rangle} (n_i - 1)(n_j - 1) \\ & - 2g \sum_{\langle i,j \rangle} \vec{S}_i \cdot \vec{S}_j \end{aligned} \quad (14)$$

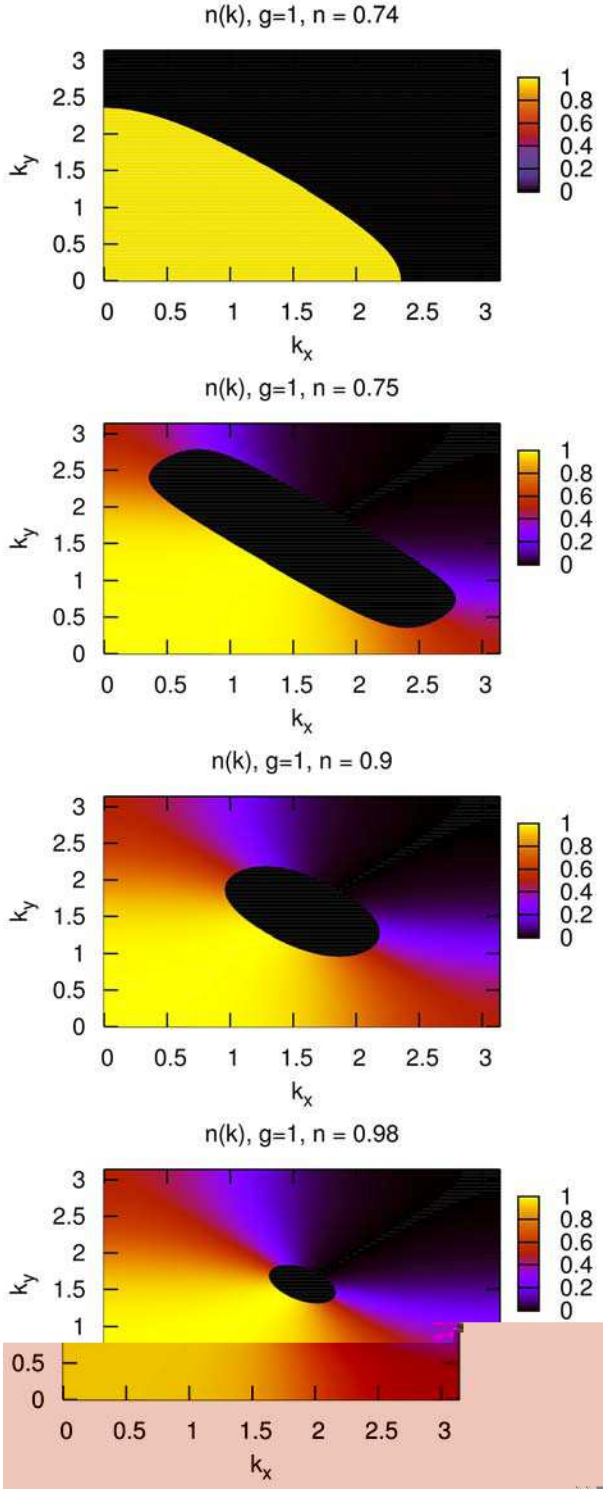


FIG. 2: (Color online) Mean-field solution of $n(\vec{k})$ over the Brillouin zone as a function of band filling for a fixed $g = 1$.

As apparent, there is a pair-hopping term so that we can expect an on-site superconducting instability which we pick up by measuring the equal time pair correlation

functions:

$$SC(\vec{R}) = \langle c_{\vec{R}\uparrow}^\dagger c_{\vec{R}\downarrow}^\dagger c_{0\downarrow} c_{0\uparrow} \rangle. \quad (15)$$

In the presence of long range off-diagonal order, its Fourier transform at $\vec{Q} = (0, 0)$

$$SC(\vec{Q} = (0, 0)) = \frac{1}{L^2} \sum_{\vec{R}} SC(\vec{R}) \quad (16)$$

should converge to a finite value in the thermodynamic limit, whereas it vanishes as $1/L^2$ in the absence of long-range order.

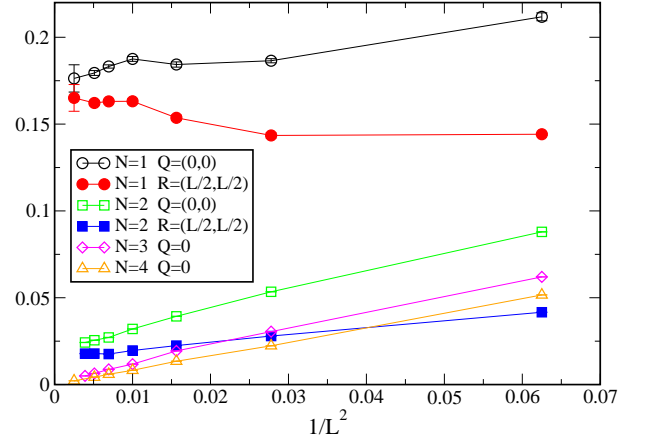


FIG. 3: (Color online) Finite-size scaling of the superconducting correlations vs the inverse number of sites $1/L^2$ of the system (L is the linear size) for the half-filled case and different N . The $\vec{Q} = (0, 0)$ Fourier correlations are plotted (open symbols) and, when long range order is present, we also show the largest distance real-space correlations (filled symbols).

The order parameter of the spin flux phase expected in the limit of $N \rightarrow \infty$, reads:

$$\langle \left[\vec{J}^s(\vec{R}, \vec{R} + \vec{x}) - \vec{J}^s(\vec{R}, \vec{R} + \vec{y}) \right] \cdot \left[\vec{J}^s(\vec{0}, \vec{0} + \vec{x}) - \vec{J}^s(\vec{0}, \vec{0} + \vec{y}) \right] \rangle \quad (17)$$

where

$$\vec{J}^s(\vec{R}, \vec{R} + \vec{x}) = i \left[c_{\vec{R}, \mu}^\dagger \vec{\sigma}_{\mu\nu} c_{\vec{R} + \vec{x}, \nu} - c_{\vec{R} + \vec{x}, \mu}^\dagger \vec{\sigma}_{\mu\nu} c_{\vec{R}, \nu} \right] \quad (18)$$

is the bond spin current operator along x (summation over repeated indices is assumed). A similar definition holds along the y direction. As expected from the mean-field solution, we have observed that the strongest signal occurs in the d-wave symmetry channel and the Fourier transform of these correlations is maximum at $\vec{Q} = (\pi, \pi)$.

Technical details: we are able to simulate up to 20×20 square lattices with a projection parameter $\theta t = 10$. We fix $\Delta\tau = 0.1$ for the Trotter decomposition. For

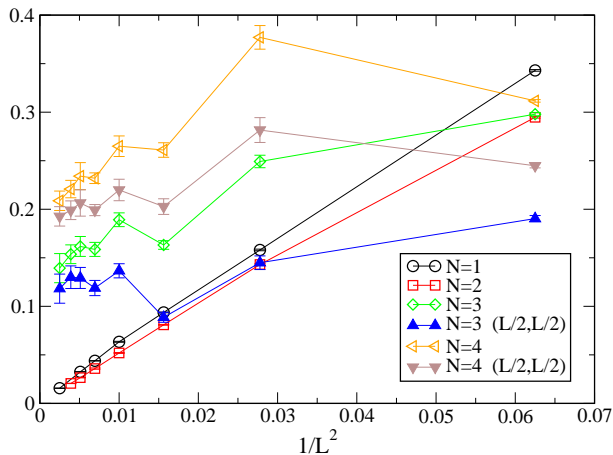


FIG. 4: (Color online) Similar as the previous plot for d -wave spin current correlations.

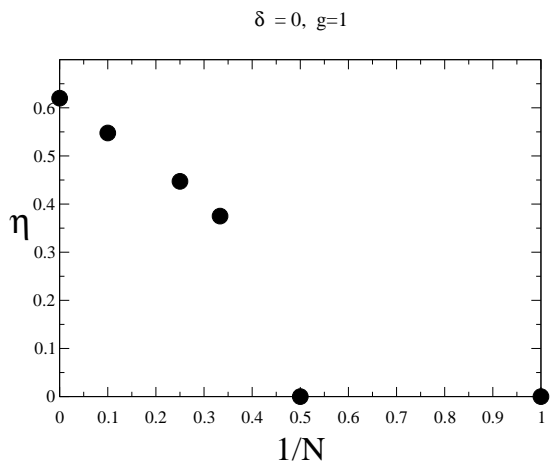


FIG. 5: Order parameter η as a function of N at half-filling. The data point at $N = \infty$ corresponds to the mean-field value.

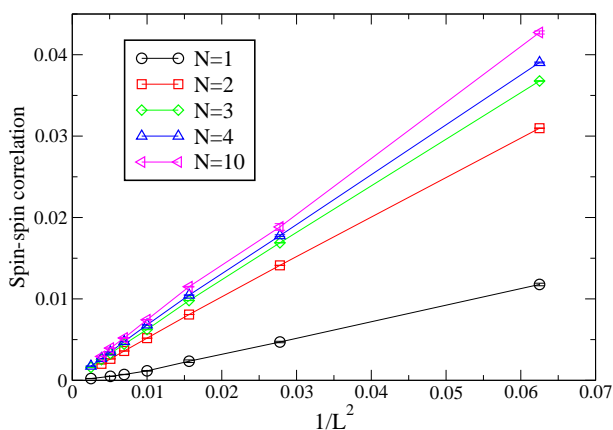


FIG. 6: (Color online) Finite-size scaling of the spin-spin correlations vs the inverse volume, $1/L^2$, of the system for the half-filled case and different N . For all cases, the $\vec{Q} = (\pi, \pi)$ Fourier correlations (which is the largest one) vanish in the thermodynamic limit, indicating the absence of magnetic order.

simplicity, in the following, we fix the coupling constant $g = 1$.

Half-filling case : On Fig. 3, we plot the scaling of the superconducting correlations for different values of N . According to our definition (16), the $\vec{Q} = (0, 0)$ correlations are divided by the number of sites so that a finite value in the thermodynamic limit indicates long range order. Moreover, when this is the case, we also plot the largest distance real-space correlations that should converge to the same value in the thermodynamic limit. In particular, we have a clear signal of s-wave superconducting phase for $N = 1$ and $N = 2$ but this phase disappears for larger N .

At $N = 1$ and under the canonical transformation,

$$c_{i,\downarrow}^\dagger \rightarrow (-1)^i c_{i,\downarrow}, \quad c_{i,\uparrow}^\dagger \rightarrow (-1)^i c_{i,\uparrow}^\dagger \quad (19)$$

the interaction term transforms as,

$$-\frac{g}{2} \left(ic_i^\dagger \bar{\sigma} c_j - ic_j^\dagger \bar{\sigma} c_i \right)^2 \rightarrow 6g \vec{S}_i \cdot \vec{S}_j - \frac{g}{2} (n_i - 1)(n_j - 1) + g(c_{i,\uparrow}^\dagger c_{i,\downarrow}^\dagger c_{j,\downarrow} c_{j,\uparrow} + h.c.), \quad (20)$$

and the kinetic energy remains invariant. The observed long-ranged pairing correlations map onto long ranged transverse spin-spin correlations. Since the transformed model has an $SU(2)$ spin symmetry, the transverse spin-spin correlations on any finite lattice take the same value as the longitudinal spin-spin correlations. Transforming back to the original model maps the longitudinal spin-spin correlations to a charge density wave order. Hence at half-filling and $N = 1$ pairing correlations and charge density wave correlations are locked in by symmetry. Clearly, doping breaks this symmetry¹⁵.

Similarly, we investigate the occurrence of SFP phase by computing the corresponding correlations (see Eq. (17)). Moreover, for a finite system, the $SU(2)$ symmetry of these correlations cannot be broken so that we average over the 3 components to reduce the error bars. For example, we plot on Fig. 7 (b) all three components of the SFP correlations showing that indeed $SU(2)$ symmetry is restored (within the error bars) despite being explicitly broken for a given Hubbard-Stratonovitch configuration. On Fig. 4, we plot the scaling of these correlations showing that SFP is present in the thermodynamic limit for $N \geq 3$ but is not stable for smaller values of N . Again, when the $\vec{Q} = (\pi, \pi)$ Fourier component indicates long range order (LRO), we also plot the scaling of the largest distance correlations that should have the same value in the thermodynamic limit for an ordered phase. In particular, we recover the existence of SFP phase for large N as found at the mean-field level. A non trivial result is that this phase survives for *finite* $N \geq 3$ since our QMC simulations, which are free of the sign problem, include quantum fluctuations. We observe rather strong finite size effects and in particular, the signal is weaker when the lattice contains $(\pi/2, \pi/2)$ k-points in its Brillouin zone. Indeed, as we will discuss in the following, this point correspond to the low-energy excitations.

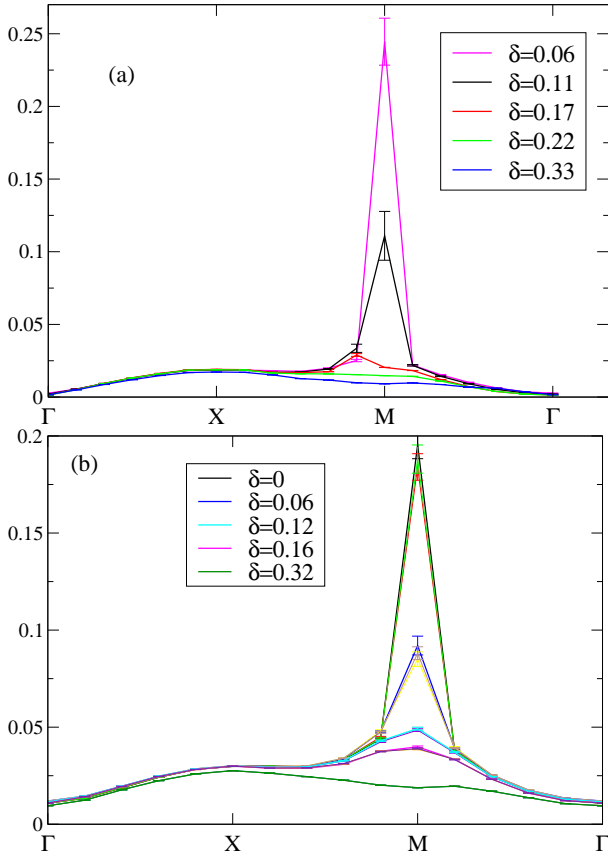


FIG. 7: (Color online) (a) Spin current correlations, averaged over the 3 components, vs \vec{k} along the (ΓXM) path in the Brillouin zone. Parameters are $L = 12$, $N = 10$ and $g = 1$. As a function of doping δ (increasing from top to bottom), the maximum at (π, π) is rapidly suppressed. (b) Same for $L = 10$ and $N = 3$. Here, we plot all 3 components showing that $SU(2)$ symmetry is recovered in our data. As a function of doping (increasing from top to bottom), the maximum at (π, π) is rapidly suppressed.

Since the staggered spin current correlation function of Fig. 4 converges to the square of the order parameter η , we can extract this quantity as a function of N . Our results are plotted in Fig. 5. As apparent, the Monte Carlo results at finite values of N smoothly scale to the mean field result valid at $N = \infty$.

In the SFP at $N \geq 3$, we have computed the spin-spin correlation functions $\langle \vec{S}_i \cdot \vec{S}_j \rangle$. As shown on Fig. 6, our results show no sign of long-range spin ordering and hence the absence of a magnetic moment. This confirms the point of view that the spin-flux phase that we observe for $N \geq 3$ indeed corresponds to a *spin nematic phase*.

Doping : Since the SFP instability occurs in the particle-hole channel, it is favored at half-filling where the Fermi surface exhibits perfect nesting. But the question about its existence under doping remains open. Our QMC simulation being free of the sign-problem for any filling, we have computed the phase diagram as a function of doping for different values of N . As expected

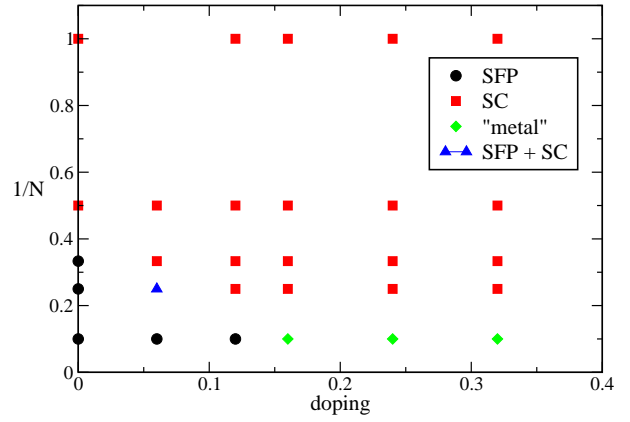


FIG. 8: (Color online) Phase diagram as a function of doping and $1/N$ obtained with QMC simulations. At large N , we recover the existence of a spin flux phase (SFP) over a finite doping region. For larger doping or smaller N , the system develops s-wave superconducting correlations (SC) or stays in a metallic phase (see text).

from the mean-field results, we show on Fig. 8 that the SFP phase has a finite extension up to a critical doping. In particular, when $N = 10$, we find a critical doping around 0.15.

On Fig. 7, we plot the spin current correlations vs \vec{k} along the (ΓXM) path in the Brillouin zone (shown in Fig. 9). For doping δ smaller than a critical value, we see a large maximum at (π, π) , whereas for larger doping, the correlations become featureless, indicating the disappearance of SFP order. We also observe that the maximum of the spin-current correlations move away from (π, π) : for example, when $L = 12$, $N = 10$ and with doping ~ 0.17 , the maximum is at $(5\pi/6, \pi)$ and equivalent k-points.

By performing a finite-size scaling analysis of our data, we are able to draw conclusion about the existence or not of a SFP in the thermodynamic limit as a function of doping and N . These results are summarized in the phase diagram shown in Fig. 8. Several comments are in order :
i) Under doping the SFP only survives for large values of N , hence showing that it is very sensitive to fluctuations. At $N = 10$ the critical doping, $\delta_c \simeq 0.15$ at which the SFP vanishes is substantially smaller than the $N \rightarrow \infty$ restricted mean-field result $\delta_c \simeq 0.25$. In the vicinity of the phase transition from the SFP to the paramagnetic phase transition at $N \rightarrow \infty$, fluctuations will play an important role. Hence at large but finite values of N , substantial differences can be expected. Furthermore, our restricted mean-field solution does not allow for incommensurate ordering as suggested by the Monte Carlo results.

ii) The rest of the phase diagram is dominated by an s-wave SC phase. At $N = 1$, the s-wave SC persists of course away from half-filling since it is a particle-particle instability that does not require any nesting property. As N grows, the s-wave SC order parameter is reduced and ultimately vanishes to produce the paramagnetic phase

in the $N \rightarrow \infty$ limit. At $N = 10$ and $\delta > \delta_c \simeq 0.15$ we observe no SFP correlations and no SC correlations either. Therefore, it seems that we might have a metallic phase with a Fermi surface. However, due to the presence of pair hopping in the model, we know that this metallic phase will ultimately be unstable at very low temperature toward s-wave superconductivity. This instability probably occurs at too low temperature to be observed in our simulations. To confirm this point of view, let us write the interaction term as:

$$-\frac{g}{2N} \sum_b \left(\sum_{\alpha=1}^N \vec{J}_{b,\alpha}^s \right)^2 = -\frac{g}{2} \sum_b \sum_{\beta=1}^N \left[\left(\frac{1}{N} \sum_{\alpha \neq \beta} \vec{J}_{b,\alpha}^s \right) \vec{J}_{b,\beta}^s + \frac{1}{N} \vec{J}_{b,\beta}^s \cdot \vec{J}_{b,\beta}^s \right] \quad (21)$$

where $b = \langle \vec{i}, \vec{j} \rangle$ denotes a nearest neighbor bond, and $\vec{J}_{b,\alpha}^s$ is the spin current on bond b for flavor index α . This forms shows that in the large- N limit, the flavor index β is embedded in the *mean field* spin current of the other flavors, $\frac{1}{N} \sum_{\alpha \neq \beta} \vec{J}_{b,\alpha}^s$. The second term, $\frac{1}{N} \vec{J}_{b,\beta}^s \cdot \vec{J}_{b,\beta}^s$ is a factor $1/N$ smaller than the *mean-field* term and provides the pair hopping term as explicitly shown in Eq. (14). At $N = \infty$, only the mean-field term survives. For large but finite values of N , a small pairing term is present and will in the paramagnetic phase trigger a superconducting instability at low temperatures.

iii) The coexistence a spin flux phase and superconductivity at finite doping cannot be excluded. As we will see below, doping the SFP leads to a Fermi surface consisting of hole pockets centered around the $(\pm\pi/2, \pm\pi/2)$ points in the Brillouin zone. Due to the presence of pair hopping, this Fermi surface should be unstable towards a superconducting state. As a result, for intermediate values of N such that we observe SFP at zero doping and such that the superconducting signal at finite doping is not strongly reduced due to a $1/N$ factor, we have found numerical evidence that supports coexistence of both phases for small doping (for instance, $N = 4$ and $\delta \sim 0.06$ in the phase diagram).

B. Dynamical properties

To study the charge degrees of freedom, we compute the single particle spectral function $A(\vec{k}, \omega)$ which is related to the imaginary time Green function via:

$$\langle c_{\vec{k},\alpha}^\dagger(\tau) c_{\vec{k},\alpha} \rangle = \frac{1}{\pi} \int_0^\infty d\omega e^{-\tau\omega} A(\vec{k}, -\omega). \quad (22)$$

In order to plot this single particle spectral function, we follow a path in the Brillouin zone shown on Fig. 9. In Fig. 10 we first plot two examples of $A(\vec{k}, \omega)$ in the SFP at half-band filling. As expected from the mean-field calculation we observe a clear sign of the Dirac cones around

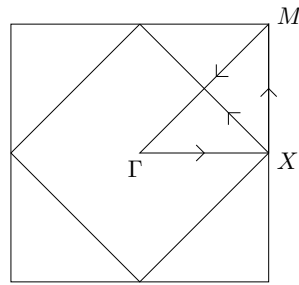


FIG. 9: In the following spectral function, from bottom to top, the k value follows the path Γ , X , M and then, along the $(\pi, 0)$ to $(0, \pi)$ line.

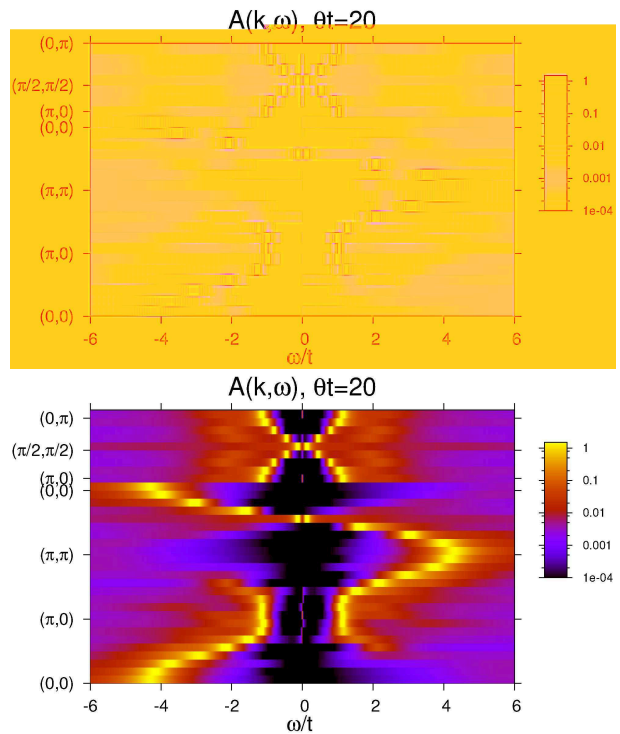


FIG. 10: (Color online) Spectral functions vs frequency ω for different \vec{k} points at half-filling. Up: $N = 10$ and $L = 12$; bottom: $N = 4$ and $L = 16$. Both set of parameters correspond to SFP and Dirac cones around $(\pi/2, \pi/2)$ are clearly seen.

the $(\pi/2, \pi/2)$ \vec{k} -points in the Brillouin zone. The overall dispersion relation compares favorably to the mean-field result

$$E(\vec{k}) = \pm \sqrt{\varepsilon^2(\vec{k}) + \Delta^2(\vec{k})} \quad (23)$$

with $\Delta(\vec{k}) = 2g\eta(\cos(k_x) - \cos(k_y))$.

In order to be more quantitative, we plot the dispersion relation of the main branch (by looking at the maximum of the spectral function) as a function of the distance to the nodal point. On Fig. 11, we clearly see the Dirac cone structure with different velocities parallel and perpendicular

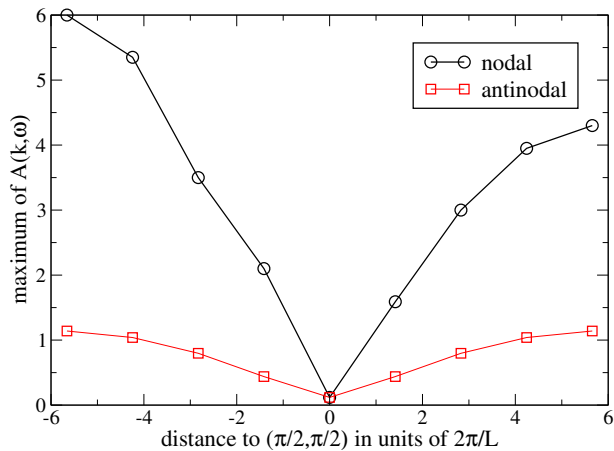


FIG. 11: (Color online) Dispersion relation obtained with $N = 4$ and $L = 16$ at half-filling. The energy is taken at the maximum of the spectral function and data are plotted vs distance to $(\pi/2, \pi/2)$. The small asymmetry is due to the uncertainty in the spectral functions obtained with a Maximum Entropy technique.

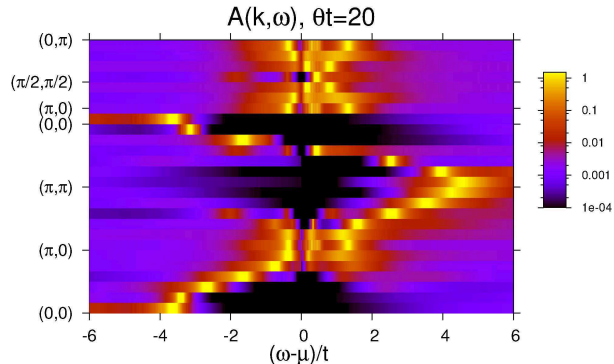


FIG. 12: (Color online) Spectral functions vs $\omega - \mu$ for different k points. Parameters are: $N = 10$, $L = 12$ and doping 0.12. It corresponds to a doped SFP phase and Dirac cones around $(\pi/2, \pi/2)$ are clearly seen. The chemical potential is $\mu = -0.48$.

ular to the Fermi surface. By fitting the slopes, we obtain for this set of parameters, $v_{\perp} = 3.11$ and $v_{\parallel} = 0.578$. At the mean-field level, according to Eq. (23), these two velocities are equal respectively to $2\sqrt{2}$ and $2\sqrt{2}g\eta$ so that their ratio gives directly access to the SFP order parameter η (when $g = 1$). Of course, the QMC data include some renormalization of these values and the ratio of $v_{\parallel}/v_{\perp} = 0.186$ is inconsistent with the SFP order parameter ($\eta \simeq 0.45$) as extracted from the spin current correlations (see Fig. 4).

In the mean-field approach, doping the SFP leads to hole pockets centered around the $(\pi/2, \pi/2)$ \vec{k} -points. Numerical QMC simulations confirms this as shown on Fig. 12. At $N = 10$ and $\delta = 0.12$ we observe a clear signature of the Dirac cone, however the quasiparticle at $\vec{k} = (\pi/2, \pi/2)$ lies above the Fermi energy.

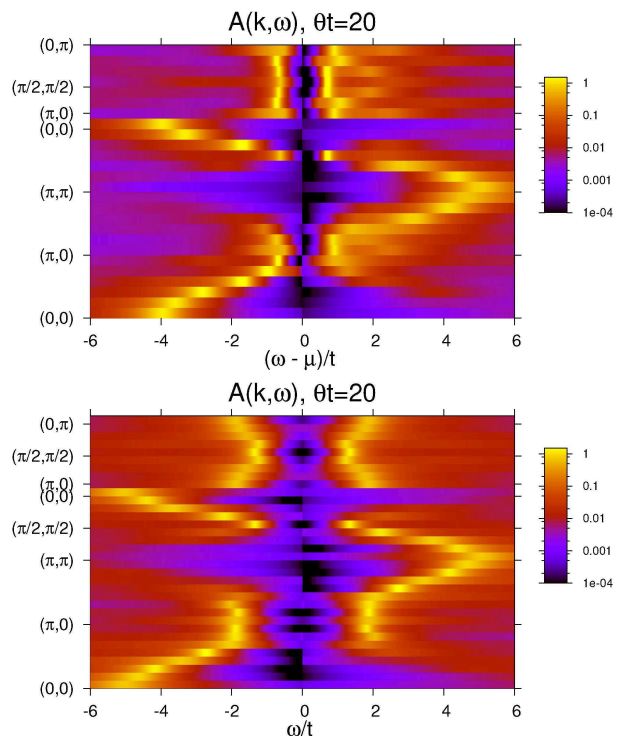


FIG. 13: (Color online) Spectral functions vs frequency ω for different k points. Top: $N = 3$ and $L = 12$ for doping 0.12 ($\mu = -0.7$). Bottom $N = 2$ and $L = 16$ at half-filling ($\mu = 0$). Both set of parameters correspond to s-wave superconducting phase.

Deep in the superconducting phase, the single particle dispersion relation follows the the mean-field form:

$$E(\vec{k}) = \pm \sqrt{(\epsilon(k) - \mu)^2 + \Delta_{sc}^2} \quad (24)$$

with k -independent superconducting gap. Such a dispersion relation is consistent with the Monte Carlo data of Fig. 13 at $N = 3$ and $\delta = 0.12$. In the proximity of the SFP at $N = 2$ and half-band filling (see Fig. 13) the dispersion is not captured by the above form. In particular, a modulation of the gap along the $(\pi, 0)$ to $(0, \pi)$ line is observed. This modulation is reminiscent of the Dirac cone structure observed in the spin-flux phase, and hence allows the interpretation that short range spin currents survive in the superconducting state in the proximity of the SFP.

IV. CONCLUSION

We have shown the existence of a spin nematic phase in a two-dimensional electronic model. This phase had been proposed at the mean-field level and it is the aim of this article to investigate its stability against quantum fluctuations. In order to do so, we have performed unbiased QMC simulations (without sign problem) for a variety of models with a flavor parameter N . With this

trick, we can interpolate from the large N limit where the mean-field is valid to finite N regime where quantum fluctuations around the saddle point are progressively taken into account. We find that the spin-flux phase is stable for a range of finite N but is ultimately destroyed for the more realistic $N = 1$ case. This is one of the few examples where QMC simulations are able to show how quantum fluctuations can destroy a large- N phase¹³. Since our model includes pair hopping processes, when the spin-flux phase is found to be unstable, it is replaced by an on-site s -wave superconductivity.

We have also investigated the phase diagram as a function of doping since our QMC simulations are free of the sign problem for any filling. Because the spin-flux phase is due to the nesting property of the Fermi surface, it is expected to disappear with doping. This is indeed what we found but still, this phase can persist over a finite range of doping, similarly to what is found at the mean-

field level.

Using a recently developed analytical continuation technique, we have computed dynamical spectral functions. In the SFP phase, we clearly see Dirac cones forming around $(\pi/2, \pi/2)$ and equivalent k -points, where the dispersion becomes linear. Up to a critical doping, these structures are stable so that the Fermi surface becomes pocket-like.

Acknowledgments

We would like to thank S.-C. Zhang for discussion. Financial support from the Bayerisch-Französisches Hochschulzentrum / Centre de Coopération Universitaire Franco-Bavarois is acknowledge. S. C. thanks IDRIS (Orsay, France) for use of supercomputer facilities.

¹ A. A. Nersesyan, G. I. Japaridze, and I. G. Kimeridze, *J. Phys. Condensed Matter* **3**, 3353 (1991).

² A. F. Andreev and I. A. Grishchuk, *Sov. Phys. JETP* **60**, 267 (1984).

³ N. Papanicolaou, *Nucl. Phys. B* **305**, 367 (1988).

⁴ P. Chandra, P. Coleman, and A. I. Larkin, *J. Phys.: Condens. Matter* **2**, 7933 (1990).

⁵ A. Griesmaier, J. Werner, S. Hensler, J. Stuhler, and T. Pfau, *Phys. Rev. Lett.* **94**, 160401 (2005).

⁶ L. Santos and T. Pfau, *Phys. Rev. Lett.* **96**, 190404 (2006).

⁷ R. B. Diener and T.-L. Ho, *Phys. Rev. Lett.* **96**, 190405 (2006).

⁸ H. J. Schulz, *Phys. Rev. B* **39**, 2940 (1989).

⁹ C. Wu and S. Zhang, *Phys. Rev. B* **71**, 155115 (2005).

¹⁰ S. Capponi and F. F. Assaad, *Phys. Rev. B* **63**, 155114 (2001).

¹¹ K. S. D. Beach, *cond-mat/0403055* (2004).

¹² A. Sandvik, *Phys. Rev. B* **57**, 10287 (1998).

¹³ F. F. Assaad, *Phys. Rev. B* **71**, 075103 (2005).

¹⁴ R. T. Scalettar, E. Y. Loh, J. E. Gubernatis, A. Moreo, S. R. White, D. J. Scalapino, and R. L. Sugar, *Phys. Rev. Lett.* **62**, 1407 (1989).

¹⁵ Precisely the same transformation has been used to investigate the half-filled attractive Hubbard model¹⁴.